# Asynchronous Mobilization of Shear Resistance in Slope Failures

**Elena Zabolotnii**, *Assistant Professor, Department of Civil and Environmental Engineering, Carleton University, Ottawa, Canada; email: elenazabolotnii@cunet.carleton.ca*
**Norbert R. Morgenstern**, *Distinguished Professor Emeritus, Department of Civil and Environmental Engineering, University of Alberta, Edmonton, Canada; email: norbertm@ualberta.ca*
**G. Ward Wilson**, *Professor, Department of Civil and Environmental Engineering, University of Alberta, Edmonton, Canada; email: wwilson2@ualberta.ca*

**ABSTRACT**: *This paper focuses on the case study of the 2014 embankment failure at the Mount Polley TSF in Canada to study deformation-controlled mechanisms of instability leading to the asynchronous mobilization of shear strength and causing progressive failure. Three such mechanisms were identified in this failure: strain-weakening, the delayed mobilization of shear strength in the shell owing to stiffness incompatibility, and a reduction of mobilized shear resistance in the extending regions of the slide due to loss of confinement. Changes associated with these mechanisms were identified in the numerical analysis to help diagnose the impending collapse. These are: the emergence in the strain-weakening unit of a substantive area on the brink of strain-weakening, the depletion of reserve strengths in the foundation materials, and the extension of the unit above the strain-weakening zone owing to differential shear displacements within and outside the failure zone. Safety factor calculations do not adequately capture the stability of the Mount Polley embankment in the year preceding its collapse, and limit equilibrium methods overestimate the three-dimensional stability effects present in this slope. The findings underscore the importance of adopting numerical analysis for assessing slope behavior.*

**KEYWORDS:** Mount Polley mine, strain-weakening, stiffness incompatibility, numerical analysis, deformation analysis, tailings dam failure, progressive failure

**SITE LOCATION:** Geographic Database

## INTRODUCTION

The 2014 breach of the embankment at the Mount Polley TSF in British Columbia, Canada, was caused by a deep-seated rotational-translational slide that initiated in a foundation unit where a progressive mechanism of failure had developed. The event was the subject of extensive investigations by IRP (2015), KCB (2015) and Zabolotnii (2020). This paper builds on these studies, particularly on the work by Zabolotnii (2020), to revisit several issues related to the application of conventional stability methods to slopes failing in a progressive manner, and to advance a number of alternative strategies to augment these.

### Theory

Classical geotechnical literature defines progressive failure as a class of slope problems where a decrease in stability, potentially to the point of collapse, is brought about by a localized reduction of shear strength below peak values. Historically, progressive failure has been associated almost exclusively with strain-weakening. Terzaghi (1936, 1948), Taylor (1955), Moore and Rowe (1988), Potts et al (1990), Ladd (1991), and many others highlight the potential for this mechanism of instability in slopes made of brittle materials. Owing to nonuniform distributions of strains and stresses, slopes may experience localized brittle failure followed by a reduction of shear strength, which can cause brittle failure in adjacent materials in a cascading manner.

Submitted: 30 November 2021; Published: 25 July 2022
Reference: Zabolotnii, E., Morgenstern, N. R., and Wilson G.W. (2022). Asynchronous Mobilization of Shear Resistance in Slope Failures. International Journal of Geoengineering Case Histories, Volume 6, Issue 3, pp. 54-72,
doi: 10.4417/IJGCH-06-03-03


*Figure 1. (a) Aerial diagonal view of the Polley Mine looking NNW; (b) Aerial diagonal view of the Mount Polley TSF, looking SSW. Photography courtesy of Jamie Heath, therrasaurus.ca, taken 09/05/2014, reproduced with permission, altered to add labels and enhance contrast/tone.*

After the progressive mechanism is triggered, the aggregate resistance along the shear surface is lower than the sum total of the soils' peak strengths (Ladd 1991, pp. 574-575). Slope stability methods that do not accommodate such reduction produce nonconservative safety factors. For example, limit equilibrium methods rely implicitly on the assumption of a simultaneous mobilization of shear strengths along the entire slip surface, and thus overestimate the safety factor of slopes failing progressively. Where the presence of a progressive failure mechanism is recognized, this limitation can be somewhat circumvented by adjusting the input strengths, for example through the introduction of tensile cracks (Golder and Palmer 1955), the localized application of post-peak strengths (Skempton, 1964, pp. 84-85; IRP 2015, p. 98) or by using approximative methods such as the strain compatibility technique by Ladd (1991, p. 575).

The asynchronous mobilization of peak strengths may be brought about by mechanisms other than strain-weakening. For example, slopes constructed with materials of contrasting stiffness may also fail in stages rather than at once, i.e. progressively. Marsal (1973, p. 195) notes the appreciable deformations required in rockfills to achieve a full mobilization of shear strengths, and remarks that stability analyses failing to account for these are inadequate. Marsal's comments are founded in the implicit assumption of the presence in the slopes in question of materials with dissimilar stiffness moduli, and the resulting possibility of functional failure prior to the full mobilization of shear strength in the more ductile units. The behavior described here is known in the broader discipline of engineering as *stiffness incompatibility*, also *stress-strain-incompatibility* or *SSI*, and its adverse impacts on a structure's performance are well recognized. In the geotechnical practice, while stiffness incompatibility effects have been long theorized, computational and other constraints have generally hindered our ability to demonstrate these in case studies involving large earthen structures.

Recent case studies of the Fundão and Cadia tailings dam failures (Morgenstern et al 2016; Jefferies et al 2019) report a mechanism of instability brought about by differential shear displacements in the underlying units. In both incidents, the failure of the tails upstream of the embankment was triggered by a loss of lateral confinement following the accommodation of either the horizontal extension of, or shear displacements in the underlying deposits; the resulting lateral unloading led to liquefaction.

The Mount Polley case study presents us with an opportunity of examining a failure triggered by three mechanisms of instability discussed here: strain-weakening, stiffness incompatibility, and loss of lateral confinement following shear displacements in the foundation.

**History of the Structure**

Mount Polley mine is a gold and copper mining operation managed by the MPMC. It is located in the Cariboo Region of British Columbia, Canada at the approximate coordinates 52°33'N 121°38'W. The mine is situated on glaciated terrain and is surrounded by pristine boreal forest along with a system of glacial lakes and creeks (Zabolotnii 2020, p. 75; Fig. 1).

The onsite TSF is a sidehill impoundment contained on the northwest by elevated natural ground, and elsewhere by three contiguous embankments with a total length of ~4.9km. The Perimeter Embankment encases the northeast side of the facility. The TSF was built in stages starting in 1995 (Zabolotnii 2020, p. 76). Its construction involved the gradual addition of embankment materials to elevations shown in Table 1, followed by the deposition of tailings and wastewater. The tailings pond levels were raised in step with crest elevations while maintaining a freeboard of 3-8m in the early stages, decreasing to ~2.3m immediately before the collapse (IRP 2015, Appx. G; Table 1).

A modified centerline design with a 2.0H:1.0V outer slope was initially adopted. In 2007, the outer slope was steepened to a 1.4H:1.0V inclination. This design modification, intended as temporary due to rockfill shortages, persisted until 2014. A 2013 memo from British Columbia's Ministry of Energy and Mines requiring a commitment from the mine operator to increase the safety factor, then estimated at ~1.3, to CDA's (2007; 2014) recommended value of ≥1.5, marks a shift in the TSF planning direction. In the fall of 2013, stripping works were completed in preparation for slope-flattening operations whereby a 2m-deep, 20m-wide trench was excavated at the toe of the embankment (IRP 2014, p. 72).

In July 2014, Stage 9B construction works commenced at the breach location; 2.5-4m of fill material were added to the embankment crest, bringing it to the pre-breach elevations of ~969, 970, and 969mASL in the shell, core, and beach areas, respectively.

*Table 1. The Mount Polley TSF embankment and pond elevations at the location of the breach.*

| Stage | Completed* | Embankment crest elevations (mASL)* | | | Approximate embankment height at crest (m) | Pond elevations (mASL)** |
|---|---|---|---|---|---|---|
| | | Core | Rockfill | Tailings (Beach) | | |
| 1 | 03/1997 | 934 | 934 | 934 | 4 | 922 |
| 2 | 02/2000 | 941 | 941 | 941 | 11 | 935 |
| 3 | 03/2005 | 944 | 944 | 944 | 14 | 942.5 |
| 4 | 10/2006 | 948 | 944 | 948 | 15 | 946 |
| 5 | 11/2007 | 951 | 950.5 | 951 | 21 | 949.5 |
| 6 | 08/2010 | 958 | 957.3 | 958 | 28 | 954.5 |
| 7 | 09/2011 | 960.1 | 959.9 | 960.5 | 30 | 958.5 |
| 8 | 10/2012 | 963.5 | 962.7 | 963.5 | 33 | 961 |
| 9A | 10/2013 | 967 | 966.1 | 964.5 | 36 | 964.5 |
| 9B | 08/2014*** | 970 | 969 | 969 | 40 | 966.83*** |

* From KCB 2015, Table 2.1.
** From IRP 2015, Appendix G; rounded off to closest 0.5m.
***At the time of the breach.

**Embankment Failure**

On 4 August 2014, a short section of the Perimeter Embankment at the Mount Polley TSF experienced a sudden and catastrophic breach, resulting in loss of containment and a spill of tailings and wastewater into the environment (Fig. 1b). The breach was caused by a deep-seated foundation failure whereby the soil mass underwent a largescale rotational-translational movement, resulting in a drop at crest and triggering an overtopping event. The original investigations determined that the failure initiated under undrained conditions in a ≤2m thick, slightly sensitive glaciolacustrine deposit at the base of the slide (referred to as the Upper Glaciolacustrine Unit, or Upper GLU), and that a progressive mechanism was involved (IRP 2015; KCB 2015). These conclusions were supported by mostly two-dimensional analyses summarized in Table 2, demonstrating that failure takes place when the Upper GLU's shear resistance reduces to peak or slightly post-peak undrained values. The pre-failure soil profile at the location is seen in Fig. 2a, also identifying the glaciolacustrine deposit central to the initiation of this failure as the Upper GLU. The Upper GLU's spatial extent and location relative to the embankment and slide is illustrated in Fig. 2b.

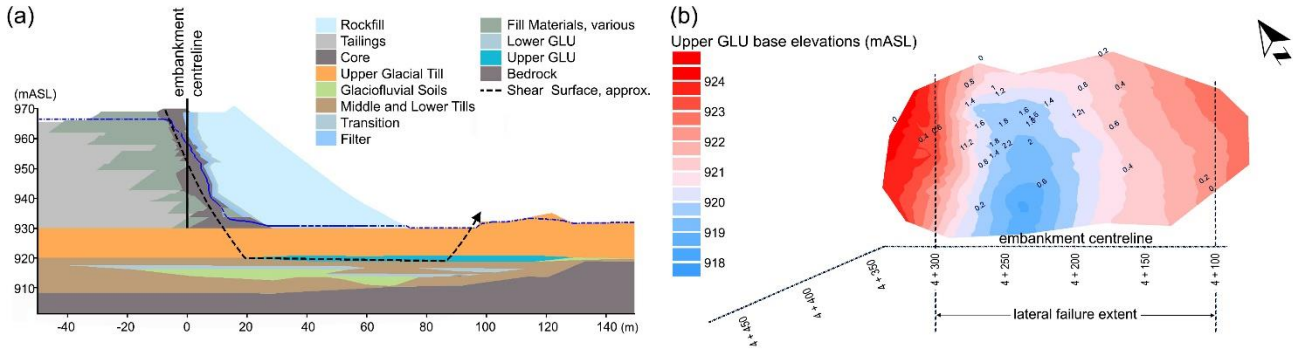


*Figure 2. (a) Pre-failure profile of embankment and foundation soils at the failure location, based on KCB's (2015) interpretation; (b) Plan view of the Upper GLU with base elevations and labeled deposit thickness (m) showing slide extent at base.*

*Table 2. Summary of stability analyses of the Mount Polley TSF embankment (pre-failure configuration).*

| No. | Completed by | Upper GLU's strength model (kPa) | Method | Notes | FS |
|---|---|---|---|---|---|
| 1 | IRP (2015) | $0.27\sigma'_{ov}$ | 2D LEM | baseline analysis, peak undrained strength | 0.991 |
| 2 | IRP (2015) | $0.22\sigma'_{ov}$ | 2D LEM | low water table, postpeak undrained strength | 1.002 |
| 3 | IRP (2015) | $0.29\sigma'_{ov}$ | 2D FEM | undrained strength reduced until failure is achieved (undrained strength at peak) | 1 |
| 4 | IRP (2015) | $0.27\sigma'_{ov}$ | 3D LEM | peak undrained strength, width-to-depth ratio=2.6 | 1.288 |
| 5 | KCB (2015) | $50+0.13\sigma'_{ov}$ | 2D LEM | baseline analysis, peak undrained strength | 1.02 |
| 6 | KCB (2015) | $36+0.11\sigma'_{ov}$ | 2D LEM | baseline analysis, postpeak undrained strength | 0.96 |
| 7 | KCB (2015) | $\sigma'_n \tan 22°$ | 2D LEM | drained strengths acting in the Upper GLU | 1.27 |
| 8 | KCB (2015) | $\sigma'_n \tan 22°$ | 2D FEM | drained strengths acting in the Upper GLU | 1.21 |
| 9 | KCB (2015) | $50+0.13\sigma'_{ov}$ | 2D FEM | baseline analysis, peak undrained strength | <1 |
| 10 | Zabolotnii (2020) | $0.18\sigma'_{ov}$ | 2D LEM | IRP's (2015) postpeak undrained strength acting in the Upper GLU | 1.021 |
| 11 | Zabolotnii (2020) | $48+0.134\sigma'_{ov}$ | 2D LEM | KCB's (2015) peak undrained strength in the Upper GLU | 1.14 |
| 12 | Zabolotnii (2020) | $36+0.122\sigma'_{ov}$ | 2D FEM | KCB's (2015) postpeak undrained strength in the Upper GLU | 1 |
| 13 | Zabolotnii (2020) | $0.27\sigma'_{ov}$ | 3D LEM | IRP's (2015) peak undrained strength in the Upper GLU | 1.31 |
| 14 | Zabolotnii (2020) | $0.18\sigma'_{ov}$ | 3D LEM | IRP's (2015) postpeak undrained strength in the Upper GLU | 1.18 |
| 15 | Zabolotnii (2020) | $0.08\sigma'_{ov}$ | 3D LEM | IRP's (2015) residual undrained strength in the Upper GLU | 1.03 |
| 16 | Zabolotnii (2020) | $48+0.134\sigma'_{ov}$ | 3D LEM | KCB's (2015) peak undrained strength in the Upper GLU | 1.313 |
| 17 | Zabolotnii (2020) | $36+0.122\sigma'_{ov}$ | 3D LEM | KCB's (2015) postpeak undrained strength in the Upper GLU | 1.254 |
| 18 | Zabolotnii (2020) | $21+0.029\sigma'_{ov}$ | 3D LEM | KCB's (2015) residual undrained strength in the Upper GLU | 1.021 |

The validity of the determinations made by the two investigations regarding the mechanism of failure at Mount Polley is challenged by the presence in this slope of substantive three-dimensional slope stability effects. Limit equilibrium analyses by IRP (2015) and Zabolotnii (2020, pp. 100-105) indicate that the three-dimensional safety factors at the failure location are greater than their two-dimensional equivalents by ~30%. The unaccounted shear resistance giving rise to these effects is generated largely in the relatively strong rockfill material forming the embankment shell. When these effects are considered together, the safety factor reduces to unity only when the average resistance in the entire Upper GLU is lowered to its undrained residual value. KCB's (2015) DSS tests on this material showing full weakening at shear strains ≥60% (seen in Fig. 3) indicate that such extensive weakening may require pre-collapse shear displacements in the order of 1.2m, if the deposit deformed uniformly. However, the lack of observable precursors to this failure rules out the possibility of such considerable deformations. Finally, ~⅓ to ½ of the Upper GLU in the failure zone was lightly overconsolidated during collapse. In this material, the response to shearing would have not been contractive, and the available resistance under undrained conditions would have been higher than the values summarized in DSS tests (Zabolotnii 2020, pp. 106-112).

To reconcile these apparent incogruities, Zabolotnii (2020) hypothesized that the initiation of this failure could be explaned by a combination of strain localization and a delayed mobilization of strength in the shell zone owing to stiffness incompatibility effects. Following extensive three-dimensional deformation analyses, Zabolotnii (2020, pp. 317-318) demonstrated that the Mount Polley failure can be triggered by a confluence of three conditions: (i) minor strain-weakening

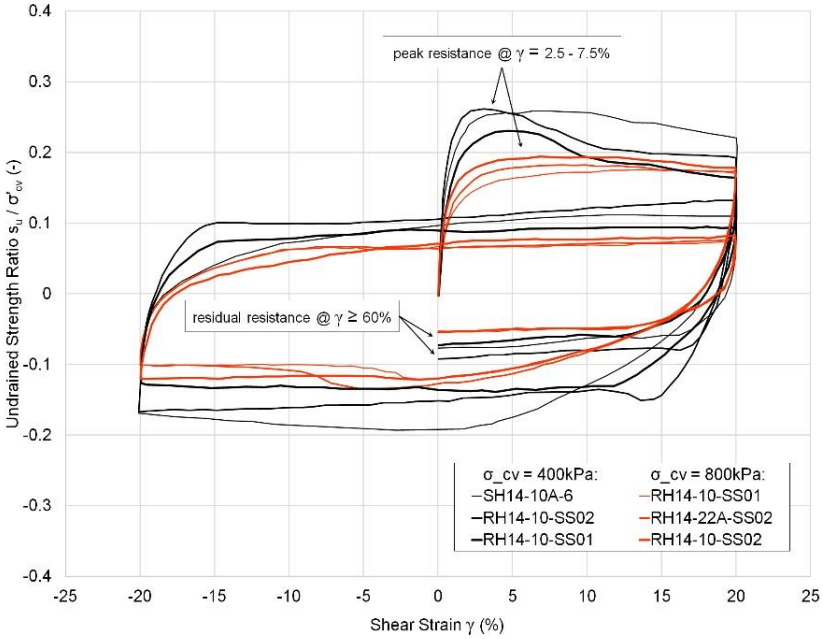


*Figure 3. Upper GLU's response to shearing in the DSS tests in the range of vertical consolidation pressures corresponding to a state of normal consolidation in this unit (based on select data adapted from KCB 2015, Fig. 5.23)*

of the Upper GLU localized to a shear band with a thickness of ~1-3cm, (ii) the asynchronous mobilization of shear resistance throughout the failing soil mass owing to stiffness incompatibility, and (iii) a sustained reduction in the levels of mobilized shearing resistance in the extending regions of the slide owing to loss of lateral confinement.

## METHOD

### Site Investigations

The two original investigations included comprehensive characterizations of the site and soils in the failure zone. Their findings, including field and laboratory testing and in-situ observations, are publicly available through their reports (IRP 2015; KCB 2015; MEM 2015, Appx. 2) and are summarized here.

The soil profile at the failure location, seen in Fig. 2a, was shaped by a complex depositional history involving three or more glaciation periods. Three distinct glacial till deposits, designated as the upper, middle, and lower tills, were separated by discontinuous interstitial deposits of glaciofluvial and glaciolacustrine provenance, including the Upper GLU, a varved deposit consisting of 1-clayey (CL-CH) layers alternating with ~1mm lamina of silt and fine sand (KCB 2015, p. 22). This deposit was located ~10m below original ground, and was spatially limited to a ~300m long, ~200m wide "pancake" with a thickness of ~2m in the middle, tapered to near-zero towards the edges. The disturbance and large shear displacements in this deposit but not below it, along with the good agreement between its spatial location and the lateral extent of slippage at base (sketched in Fig. 2b and evidenced by the ground uplift at the slide's toe, seen in Fig. 4, feature U) underscore its critical role in the failure (IRP 2015, pp. 21-22). The Upper GLU was closely examined and subjected to extensive in-situ and laboratory testing.

Prior to construction, the Upper GLU was overconsolidated with preconsolidation pressures of 400-500 kPa. Under the loads imposed by the embankment, it became normally consolidated sometime before its failure. This transition caused the deposit to become contractive and therefore susceptible to developing excess pore pressures on shearing (a failure mode commonly referred to as "undrained"). The Upper GLU was slightly sensitive with a sensitivity ≤3 and prone to strain-weakening as indicated by DSS and other laboratory tests (IRP 2015, p. 39; KCB 2015, Appx. II). No continuous pre-sheared planes were identified in this deposit. The totality of this evidence coupled with two-dimensional back-analyses invited the conclusion that the unit's contractivity and propensity to strain-weaken were the reasons for the catastrophic failure of this structure upon the addition in Stage 9B of what amounts to 3-5% of the total load imposed by the embankment.


*Figure 4. (a) Aerial diagonal view of the breach and spill path areas; (b) Aerial diagonal close-up of the breach location. Labels: C – core remnant, R – rockfill at the east boundary of the slide, U – uplift at the toe of the slide. Photography courtesy of Jamie Heath of terrasaurus.ca, taken 09/05/2014, reproduced with permission, altered to add labels.*

Above the slide base, the geometry of the slip was irregular. Extensive ground cracking, shear zones (IRP 2015, Fig. 5.1.7), and sheared remnants of core (Fig. 4, feature C) delineated the extent of the slide in the upstream region roughly along the dam centerline and just few meters upstream of the Upper GLU's upstream edge. The failure zone was restricted to a width ~100m at ground level, widening to ≤150m at crest level. The broad (200-250m) slip surface in the Upper GLU did not clearly propagate into the embankment; however, the rockfill in the shell zone flanking the breach is seen to have undergone significant deformation (Fig. 4, feature R). This material's lower deformation modulus and resulting stress-strain incompatibility with the rest of the structure was inferred both from the large deformations at failure but also from a documented history of poor compaction and low confinement stresses.

**Numerical Formulation**

The formulation of the numerical model of the Mount Polley failure is reported in full by Zabolotnii (2020, pp. 113-162). The analysis was completed in Itasca's FLAC3D software using its largestrain calculation scheme. It follows the construction history of the structure through the sequential addition of loads corresponding to Stages 3-8, 9A, and 9B, as well as the trench excavation works in Stage 9A. The Upper GLU's mechanical behavior was approximated with a semi-custom constitutive model whose undrained response, applicable upon its transition to a state of normal consolidation under the loads imposed by the embankment, was derived from DSS tests conducted on this material by KCB (2015, Fig. 5.23). The undrained response incorporates a hardening component correlated with vertical consolidation pressures, and a weakening component correlated with the accumulation of plastic shear strains. Calibration exercises produced a range of strain-weakening curves all offering a reasonable fit for the DSS testing data; the conservative interpretation, representing the most brittle response within the calibrated range was adapted in the baseline simulations, whereby the onset of strain-weakening takes place at $\gamma_s^p$=5%, and the material is fully weakened at $\gamma_s^p$ ≥60%.

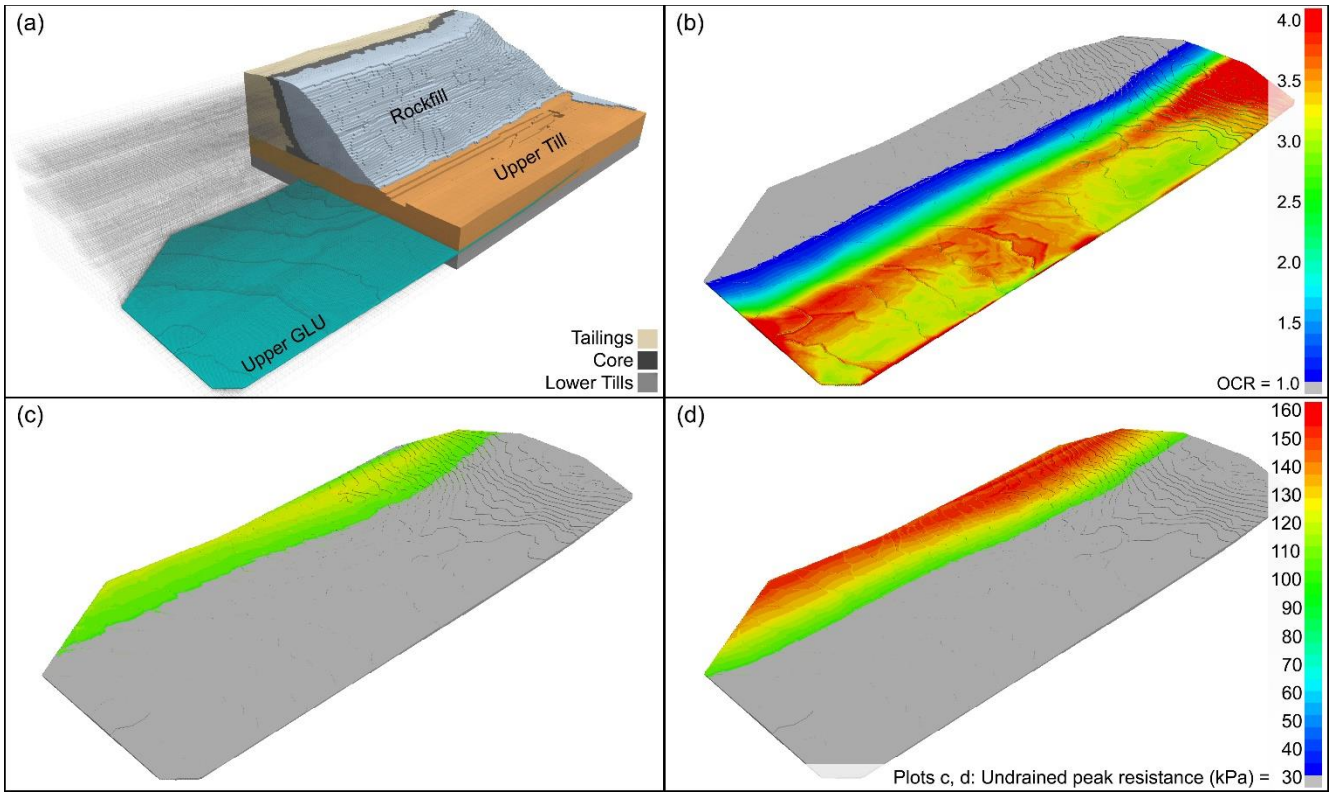


*Figure 5. (a) The three-dimensional model of the failure location in Stage 9B (pre-failure) shown in a cross-sectional view through the middle of the slide; the rest of the domain rendered as a mesh, and the Upper GLU is rendered in full; (b) View of the Upper GLU in Stage 9B showing overconsolidation ratios; the rest of the model is rendered invisible; (c), (d) Views of the Upper GLU in Stages 5 and 9B, respectively, showing peak undrained resistance in the normally consolidated zone.*

**Mesh Sensitivity**

The numerical analysis of the Mount Polley failure exhibits pronounced mesh sensitivity largely related to the nonlinear strain-weakening response in the Upper GLU. These effects were extensively investigated, with a full account of the findings along with the strategy used to evaluate them reported by Zabolotnii et al (2021). Here, it suffices to state that a composite strategy was applied, including (i) the evaluation of three models with different mesh discretization levels, (ii) the analysis of the upper and lower limit states of the model response using the method proposed by Zabolotnii et al (2021), and (iii) the examination of analytical arguments and field evidence. The results reported here are obtained from the simulation whose model equivalence to in-situ conditions was amply demonstrated.

**Safety Factor**

In numerical analyses of strain-weakening systems, safety factor calculations using the SSR method cannot be applied directly as the shear strength is a function of deformation. Zabolotnii (2020, p. 162) and Zabolotnii et al (2021) report a common modification of the SSR method whereby the strain-weakening material is converted to a Mohr-Coulomb material using the operational strength parameters prior to their multiplication by a factor of *1/FS*. While the resulting safety factors may not be meaningful in the traditional sense, they offer a means of comparing the relative response of models that differ only with respect to their mesh resolution. Additionally, once model equivalency to prototype behavior is established, safety factors obtained using this approach can be compared to values obtained by other methods. SSR safety factors reported in this paper were calculated in accordance with this method.

**RESULTS**

The model of failure at the Mount Polley TSF formulated by IRP (2015) and expanded on by Zabolotnii (2020) posits that progressive failure initiated in the Upper GLU under undrained conditions following the unit's transition to a contractive behavior under the loads imposed by the embankment. This mechanism necessitates the coevolution of a number of processes in the foundation, creating conditions promoting first strain-weakening in the Upper GLU, and later global failure. The evolution of these processes was observed in the simulation by tracking a number of key variables.

**Changes Precipitating the Initiation of Progressive Failure**

In the simulation, starting in the earliest stages of construction, the gradual addition of embankment materials triggers stress adjustments throughout the domain. Total and effective stresses rise, and, under the increasingly asymmetrical loading of the ground under the sloped portion of the embankment, stress distributions progressively deviate from the $K_0$ conditions. In the region under the core, a combination of an elevated phreatic zone, a high-density fill, and full saturation result in stress changes in the foundation below that eventually lead to the initiation of strain-weakening in the Upper GLU.

*Upper GLU's Change of Failure Mode*

In the simulation, the Upper GLU's transition from an overconsolidated to a normally consolidated state denotes a change in its mechanical response from drained to undrained. The Upper GLU material under the crest becomes normally consolidated by Stage 5. With growing embankment heights, this zone continues to expand until Stage 9A, encompassing, prior to collapse, ~¼ of its total area. The extent of the normally consolidated zone at failure is pictured in Fig. 5b.

*Hardening*

The hardening of the Upper GLU is illustrated in Fig. 5c-d. Unlike other changes in the Upper GLU described here, its consolidation-induced hardening has a beneficial effect on the stability of the structure, buffering it to some degree against failure.

*Yielding in the Upper GLU*

A region of high shear stresses develops in the core and below it (Fig. 6a). At this location, the Upper GLU, being the weakest of the units, is the first material to reach yield; this takes place as early as Stage 5. Its yielding is evidenced by the band of

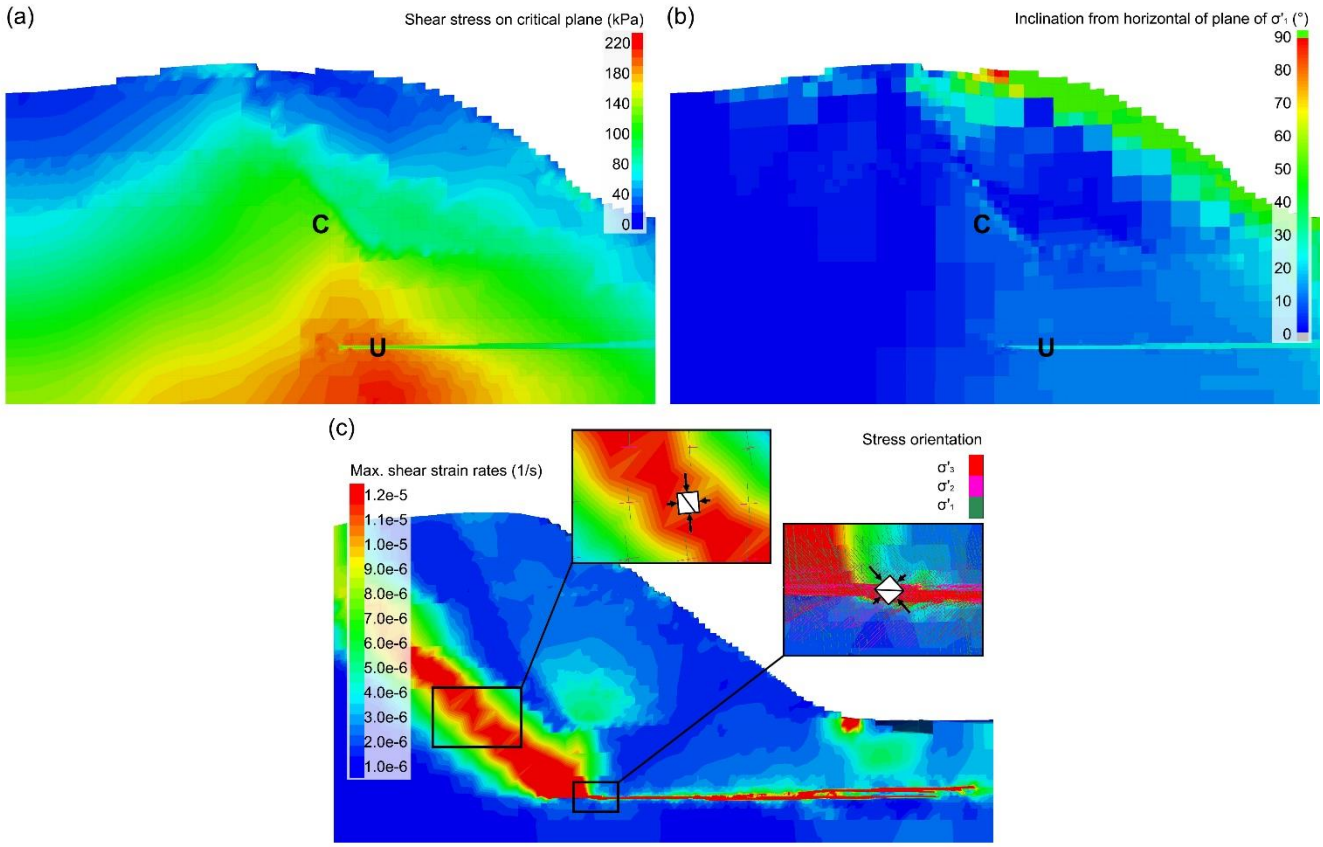


*Figure 6. A cross-sectional view through the middle of the slide showing: (a) shear stresses on the critical plane after the adjustment to Stage 6 loads; (b) the deviation from horizontal of the plane of major principal stress after the adjustment to Stage 6 loads; and (c) maximum shear strain rates, the orientation of principal stresses, and of the planes of critical stress at an advanced point of collapse in Stage 9B. Labels: C – core; U – upstream portion of the Upper GLU.*

lower shear stresses indicating that a downward adjustment had taken place within this unit. This material is mobilizing plastic shear strain.

*Rotation of Stress Tensor*

The asymmetrical loading of the ground under the slope induces a gradual rotation of the stress tensor. The major principal stresses, initially acting more or less vertically on a horizontal plane, shift to an increasingly inclined position, and the planes of critical stress rotate. By Stage 6, deviations from horizontal of the plane of major principal stress vary between 10º and 20º in the core, and between ~25º and ~40º in the Upper GLU (Fig. 6b). As a result, the maximum shear resistance is mobilized in the Upper GLU as the stresses rotate.

The reorientation of the planes of critical stress influences the position and alignment of the slip surface. This effect is illustrated in Fig. 6c, showing the inclination of principal stresses and that of the planes of critical stress at two key locations, the core and the upstream portion of the Upper GLU, superimposed on the plot of maximum shear strain rates in the cross-section through the middle of the slide at an advanced point of collapse. The plot demonstrates the good alignment of critical planes with the dominant shearing directions at large shear strains during failure. One may surmise that these processes are mirrored in situ, although confirmatory evidence is indirect in the form of matching performance as stress tensors are calculated, not measured.

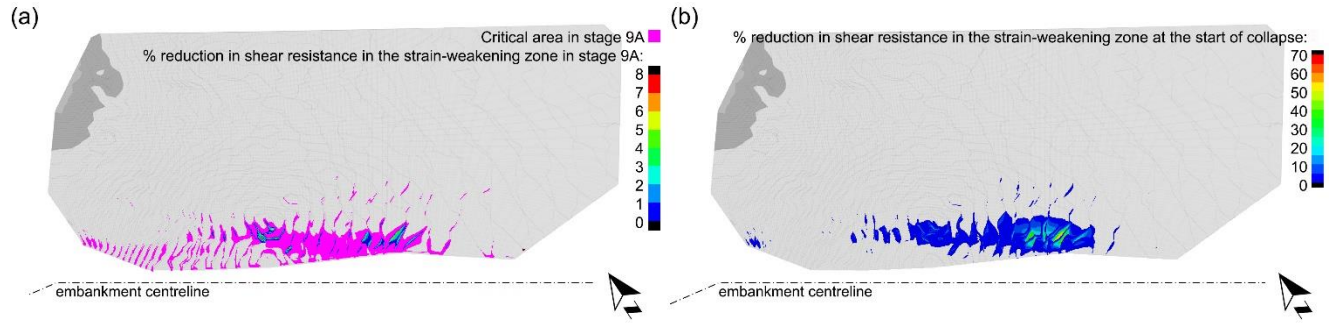


*Figure 7. Plan view of the Upper GLU. (a) The critical area and the strain-weakening zone with % strength reduction below peak in Stage 9A. (b) The strain-weakening zone at the onset of global failure with % strength reduction below peak.*

**Contained Progressive Failure**

The loading-induced changes in the foundation and embankment create a confluence of conditions requisite for the initiation of progressive failure in the Upper GLU. By Stage 6, the upstream portion of this deposit is contractive and exhibits an undrained mechanical response, is experiencing plastic yielding, and is shearing preferentially in the downstream direction. In the simulation, the progressive failure of the foundation begins in Stage 7, whereby a small region under the crest accrues plastic shear strains ≥5% and begins weakening. The strain-weakening localizes in a single row of elements at or close to the base of the deposit. The progressive failure remains contained through Stage 9A. The areal extent of the strain-weakening zone expands from <1m$^2$ in Stage 7 to ~160m$^2$ in Stage 9A (Fig. 7a). After the adjustment to Stage 9A loads, plastic shear strains in the strain-weakening zone range between 5 and 14%, averaging at 6.7% and producing an average reduction of shear resistance of 2-3% below peak undrained (Fig. 7a). With an average peak undrained strength $s_{u,peak}$≈160kPa, such a reduction amounts to a shear strength decrease of 3-5kPa.

The shearing of the strain-weakening zone is associated with a progressive accumulation of horizontal displacements in the downstream direction. By Stage 9A, displacements in the order of 12-14cm are calculated at the middle of the localization feature, coincident with the center of the slide base (Zabolotnii 2020, p. 232 & Fig. 4.42).

**Changes in the Foundation Preceding the Onset of Uncontained Progressive Failure**

The hypothesis formulated to explain the initiation of failure at Mount Polley posits that a large fraction of the Upper GLU in the failure zone, possibly its entire normally consolidated region, had experienced a reduction in its shear resistance to residual or near-residual levels prior to the start of collapse (Zabolotnii 2020, pp. 111-112). From this proposition one may conjecture that the contained progressive failure advanced considerably prior to Stage 9B. The simulation results do not corroborate this proposition: the 2-3% reduction of shear resistance below peak undrained in the plastic yield zone observed in the model in Stage 9A, corresponding to a 3-5kPa reduction of strength across an area of ~160m$^2$, is trivial at the scale of the breach and does not materially impact the immediate stability of the slope. The Stage 9A safety factor, estimated using either limit equilibrium methods or the modified SSR method, ranges between 1.3 and 1.4, values suggestive of a reasonably safe slope configuration.

In view of these findings, the onset of collapse in the simulation upon the addition of Stage 9B loads, consisting of 2.5-4m of fill in the crest region, representing ~5% of the total load imposed by the embankment, may appear surprising. Zabolotnii (2020, pp. 338-341) demonstrates that in the model, the initiation of failure in Stage 9B does not appear to be particularly sensitive to the nature of disturbance and is triggered under a variety of loading scenarios. These results lead to the conclusion that the conditions necessary for the initiation of global failure are fully realized by Stage 9A. From then on, minor perturbations can trigger it.

In the simulation, the collapse in Stage 9B is precipitated by several changes in the foundation. Three changes are identified, with the combined effect of bringing the slope to the brink of collapse in Stage 9A. These are: the emergence of a large area in the Upper GLU that is on the verge of strain-weakening, the depletion of reserve shear strengths in the foundation, and an

accumulation of shear displacements in the upper till unit above the strain-weakening area that places some of the deposit into extension.

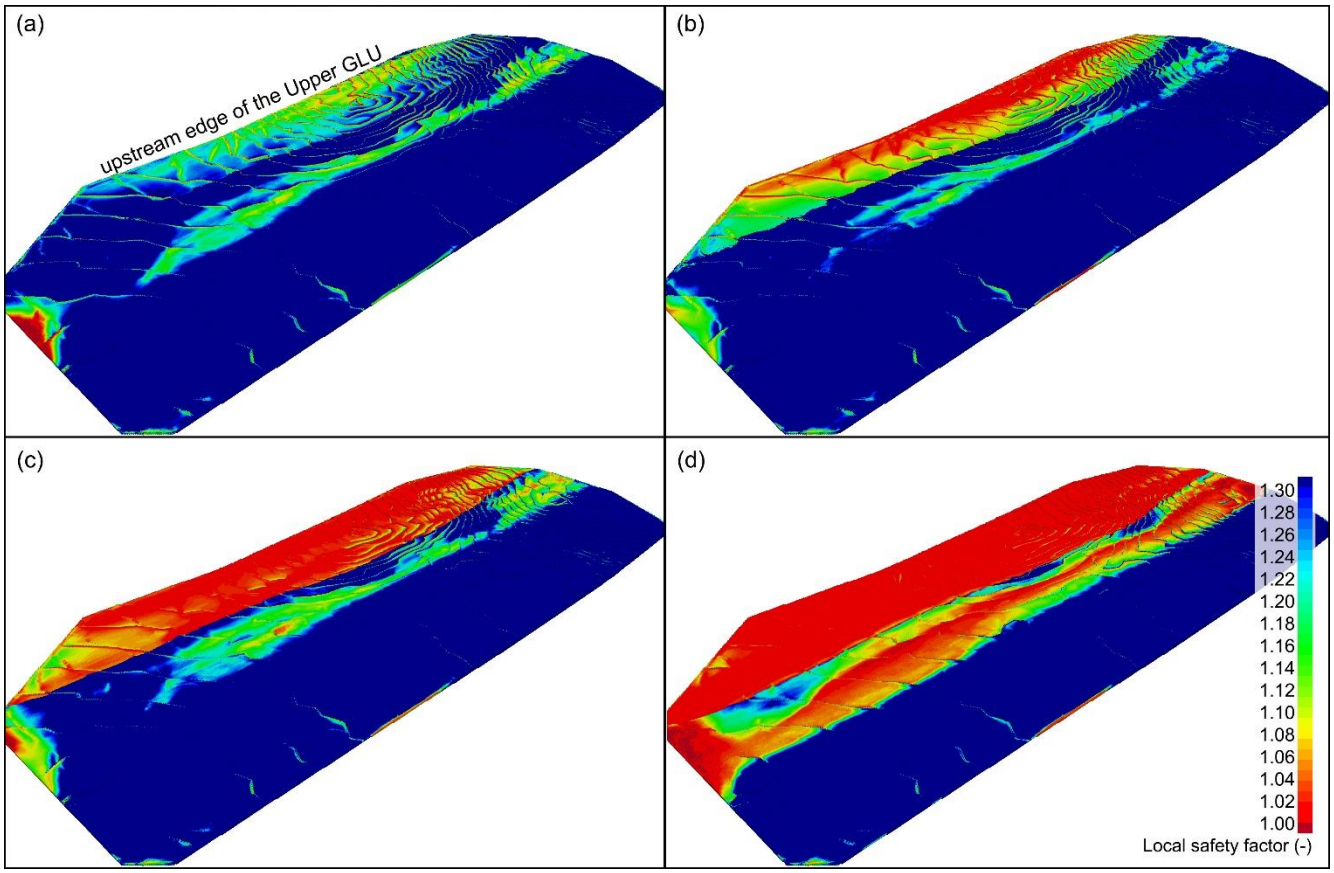


*Figure 8. Plots of local safety factors in the Upper GLU after the adjustment to loading conditions corresponding to: Stages (a) 5, (b) 6, (c) 7, and (d) 8 respectively.*

One reason why the progressive failure remains contained in Stages 7-9A is that there is a reserve of not yet mobilized shear strength present in the soil mass around the strain-weakening zone. This allows the surrounding soils to accommodate stress transfers from the strain-weakening areas. The ongoing construction of the embankment gradually depletes this reserve (Zabolotnii 2020, p. 303). This effect can be visualized by examining local safety factors, representing the ratio of shear strength $\tau_{ff}$ to mobilized shear stress along the critical plane $s_{cr}$:

$$FS_{local} = \frac{\tau_{ff}}{s_{cr}} \quad (1)$$

In Stages 5-6, local safety factors at a point in the Upper GLU material under embankment range between 1.2 and 1.3+, if edge effects at the model boundaries are ignored (Fig. 8a-b). The local safety factors decrease in each subsequent construction stage: by Stage 7, most of the normally consolidated portion of the Upper GLU is near yield, and by Stage 8, the reserve strengths in the overconsolidated portion of the deposit under the embankment are also largely depleted (Fig. 8c-d). The depletion of reserve strengths is more pronounced at the base of the deposit and immediately downstream of the emerging shear band. By Stage 9A, the lightly overconsolidated material adjacent the normally consolidated zone is also at yield (Zabolotnii 2020, Fig. 6.7).

In a coupled process, a large portion of the Upper GLU under the core accrues sufficient plastic shear strains to approach the brink of loss of stress resistance due to stress path effects (Zabolotnii 2020, pp. 242, 305). The footprint of this critical area

after the adjustment to Stage 9A loads is estimated at 4,000-6,000m$^2$ (Fig. 7a). This material engulfs the strain-weakening zone.

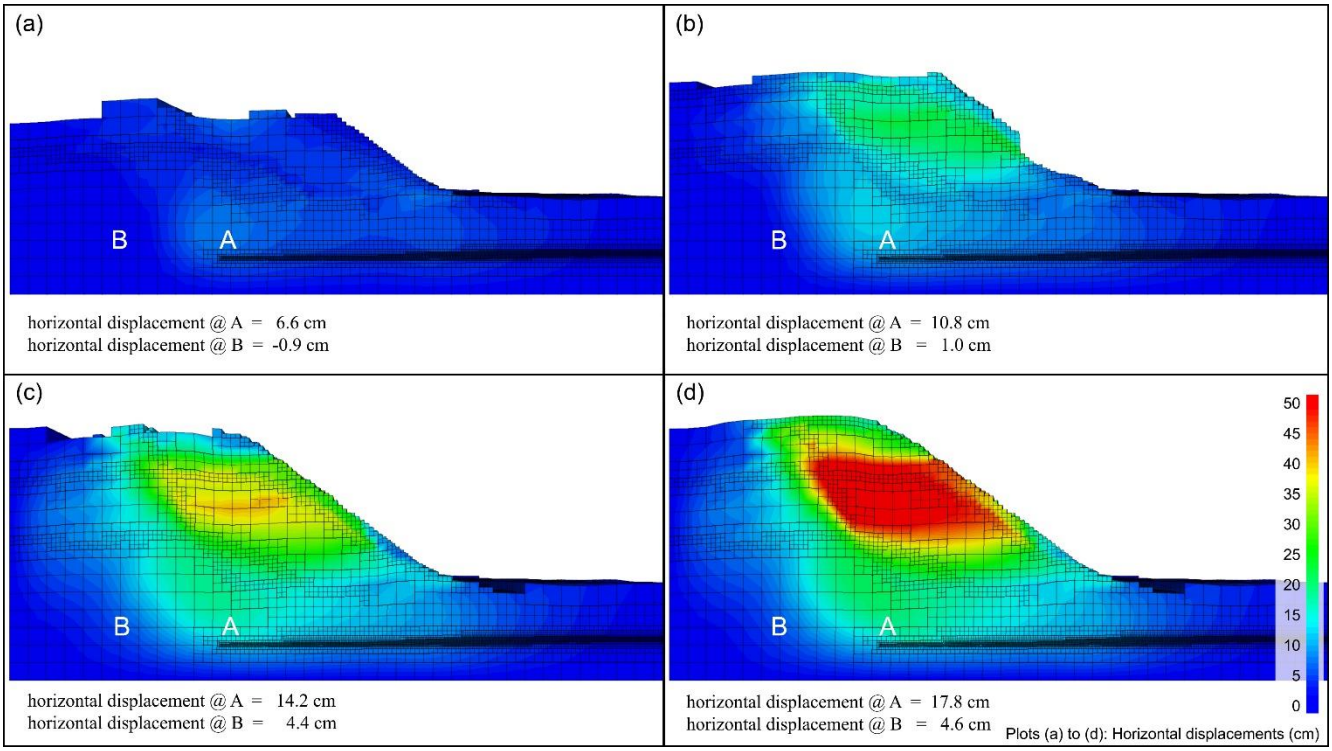


*Figure 9. A cross-sectional view of the fine model through the middle of the slide showing horizontal displacements in the downstream direction in Stages (a) 5, (b) 7, (c) 9A, and (d) 9B at the start of Phase II. Labels: A – the upper till above the strain-weakening zone; and B – the upper till on the upstream of the slide (adapted with permission from Zabolotnii 2020, Figure 6.11).*

Finally, ongoing plastic processes in the Upper GLU cause an accumulation of shear displacements in this region, predominantly in the downstream direction. Starting around Stage 7, the upper glacial till deposit located directly above the Upper GLU carried with it. Figure 9 illustrates the horizontal displacements in the downstream direction of the slide at its mid-point. Point A, located in the upper till above the strain-weakening zone in the upstream region of the slide, displaces by ~6.6cm in Stage 5 (Fig. 9a), and by ~14.2cm in Stage 9A (Fig. 9c); in contrast, point B, located in the upper till immediately upstream of the failing soil mass, is displacing considerably less. These displacements suggest that, to accommodate the growing shear displacements in the foundation, the upper till is extending. In the figure, the horizontal displacements in the upstream region of the slide (point A) increase from ~7cm in Stage 5 to ~14cm in Stage 9A.

**Global Failure**

In the simulation, global failure develops after the addition of Stage 9B loads. The failure unfolds in a specific sequence of events, as documented by Zabolotnii (2020, §6.1). This sequence is revisited here in the context of findings discussed in the previous section.

After the addition of Stage 9B loads, the foundation materials, already at yield, respond by straining. The critical area begins strain-weakening, causing an upsurge in the rate of loss of shear resistance. The broader Upper GLU deposit surrounding the strain-weakening zone, also at yield, is now readily accumulating plastic shear strains approaching the onset of strain-weakening. Associated with the increase in the rate of strain-weakening is a renewed accumulation of shear displacements in the downstream direction. The glacial till above it continues to accommodate these displacements until 500-3,000 mechanical steps into the simulation; at this point, the differential horizontal displacements in this unit above the strain-weakening zone increase to ~14-18cm, up from 12-14cm prior to the addition of new loads (Fig. 9c-d).

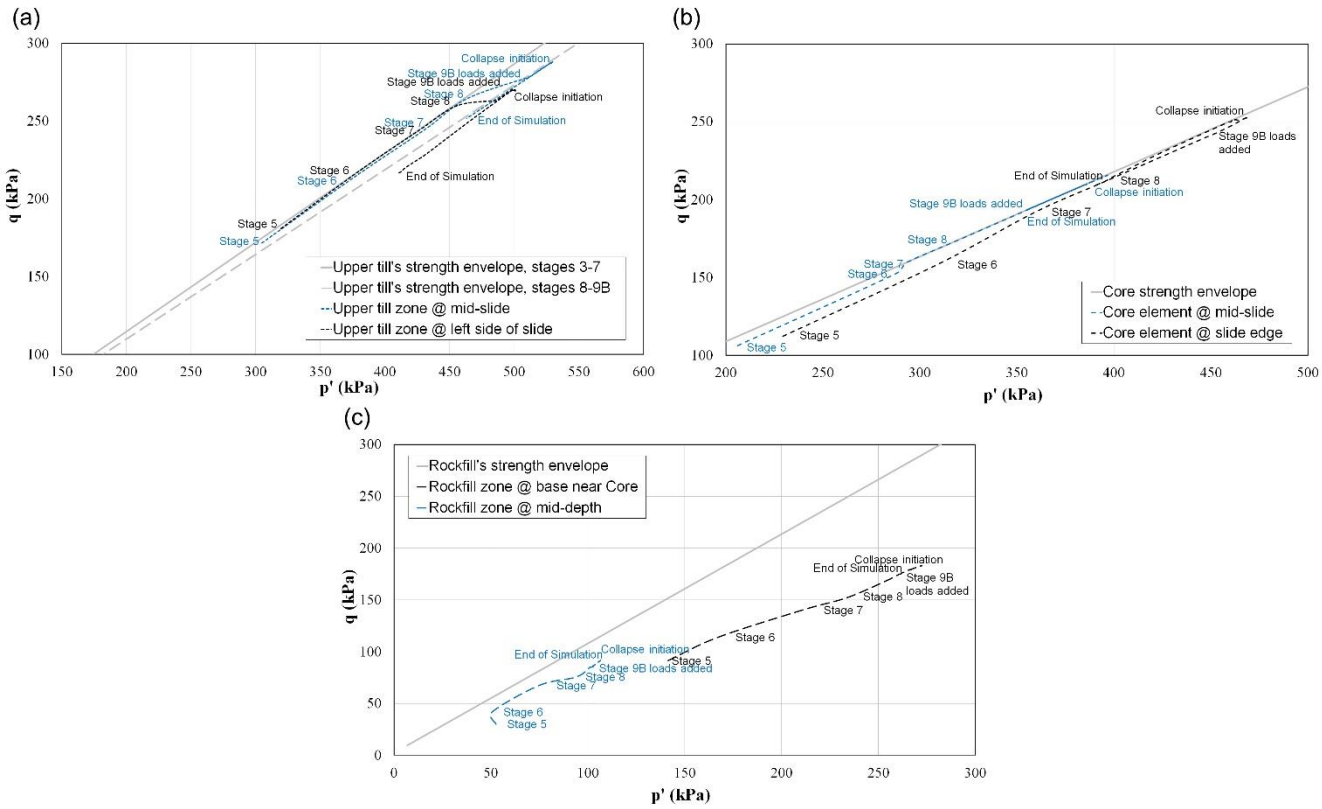


*Figure 10. (a,b,c) Stress states in representative elements of the upper till and core materials in the upstream regions of the slide, and in the rockfill, respectively.*

About 500-3,000 mechanical calculation steps after the addition of Stage 9B loads (depending on the location in the failing soil mass), the stress response in the till unit changes qualitatively: in this region, the effective stress states, which until this point were experiencing a steady increase in response to growing loads, are now decreasing owing to a relaxation of confining stresses. This produces, among other things, a gradual reduction in the levels of mobilized shear resistance acting along the planes of critical stress in this region. This effect is seen in Fig. 10a, illustrating the stress responses recorded at two representative locations in the upper till, one at the slide mid-point another ~30m south-east of it. At these points, the stress states increase consistently throughout the simulation in response to the loads imposed by the newly added embankment materials, until shortly after the addition of Stage 9B loads when the stress states begin steadily decreasing. This process sets in earlier at the slide mid-point, located directly above the middle of the strain-weakening zone, and later at the point located further away from the slide epicenter.

In the simulation, the reversals of the upward trends of the stress states in the upper till coincide with the moments when the shear surface propagates into the upper till at those locations. This effect can be appreciated from Fig. 11a. Fig. 11 displays the plots of the zones that are experiencing markedly higher shear strain rates than the rest of the modeled domain, thus offering a visualization of the shear surface at a specific point of the simulation. Fig. 11a captures the shear surface at a moment 2,700 mechanical steps after the addition of Stage 9B loads; the horizontal planar surface (speckled with red hues) is located in the Upper GLU, providing an indication of the failure processes at the base of the slide, while the sloping wedge above it, labeled "S," is located in the upper till directly above the location where the strain-weakening zone first emerged.

The qualitative change in the stress response of the upper till in the upstream region of the slide precedes the moment when global failure develops in the simulation, evidenced by the overall acceleration of the soil mass ~3,000 mechanical steps into the simulation of Stage 9B (Zabolotnii 2020, p. 313 & Fig. 4.41). At this point in the simulation, the rate of loss of shear resistance to strain-weakening has increased ~30-fold. The rate of accumulation of shear displacements at the middle of the strain-weakening zone increases three- to fourfold (Zabolotnii 2020, p. 309 & Fig. 6.12). The growing shear displacements in the foundation drive the shear surface upward into the core as well as laterally, as seen in Fig. 11b-c. The change in the

stress response noted previously in the upper till is also observed in the core in step with the propagation of the shear surface (Fig. 10b).

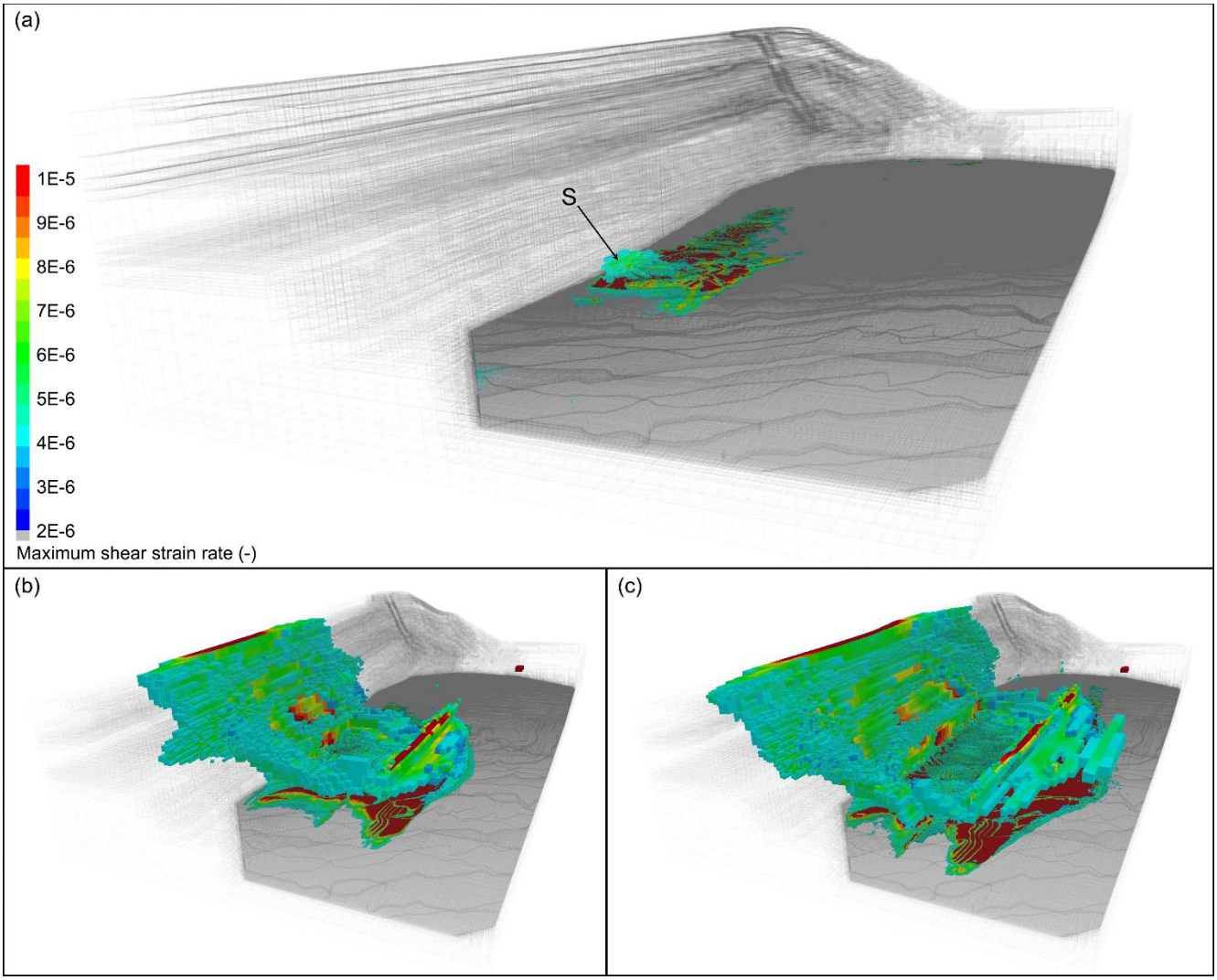


*Figure 11. (a,b,c) Shear surface 2,700, 5,200 and 6,700 mechanical steps after the application of Stage 9B loads, respectively. Elements with maximum shear rates ranging between $2*10^{-6}$ and $10^{-5}$(-) are rendered in color; all other zones are shown as transparent mesh. Labels: S – location where the shear surface propagates outside the Upper GLU and into the upper till at ~2,700 mechanical steps into the simulation of Stage 9B.*

The rockfill in the shell zone exhibits a manifestly different mechanical response. Since the start of simulation, this material experiences stress states plotting well below its strength envelope. The plots in Fig. 10c demonstrate that during the collapse, the stress states in this material experience a modest increase, and that the shear strength of this material is not fully mobilized at any point.

## DISCUSSION

The back-analysis of the Mount Polley case study by Zabolotnii (2020) suggests that the mechanisms responsible for triggering the embankment collapse were deformation-controlled and produced a distinctly asynchronous mobilization of shear resistance in the failing soil mass. The case study presented here showcases the value of deformation analysis residing with its ability to capture the stress path of a structure and, in doing so, to offer clues about the risks of instability associated

with credible stress paths. In this section, the Mount Polley case study is used to explore some of the strategies to mine for indicators of potential instability that emerge prior to generalized failure in a numerical analysis whose equivalence to prototype behavior has been established. In the case of Mount Polley, such equivalence was established by matching the observational history both prior to and during the collapse (Zabolotnii 2020). Other case histories such as that of the Alameda Dam (Quinn et al 2014) demonstrate that such equivalence can be successfully established for stable structures by history-matching monitoring data.

**Mechanisms of Asynchronous Mobilization of Shear Resistance**

The study by Zabolotnii (2020) establishes that the sudden collapse of the Mount Polley embankment during the night of 4 August 2014 was triggered by a confluence of three conditions: a modest reduction of shear resistance in the foundation, the incomplete mobilization of shear strength in the shell zone, and a reduction in the levels of mobilized shear resistance in the extending regions of the slide. Three distinct mechanisms were involved: the loss of shear strength due to strain-weakening, the differential mobilization of shear strengths owing to stiffness incompatibility, and the downward adjustment of stresses brought about by loss of confinement.

*Strain-Weakening*

In the Mount Polley numerical analysis, the onset of global failure is precipitated by a surge in the aggregate rate of loss of shear resistance to strain-weakening largely owing to a ~30-fold areal expansion of the strain-weakening zone. The expansion of this zone after the application of Stage 9B loads is illustrated in Fig. 7, showing side-by-side its areal extent at the end of Stage 9A and at the onset of global failure. The figure showcases the good agreement between the locations of the critical area in Stage 9A and the strain-weakening zone at the onset of global failure.

The substantial size of the critical area on the brink of weakening in Stage 9A suggests that the extent of strain-weakening is about to increase dramatically in response to minor added loads. This impending surge is not captured by conventional stability methods (including limit equilibrium methods and the modified SSR method) which rely on operational shear strengths along a prescribed stress path and thus produce safety factors suggestive of much safer configurations than warranted by the metastable state of this slope. Therefore, when dealing with strain-weakening systems, it may be of use to monitor the state of the strain-weakening unit to detect the potential for impending changes in the extent of loss of shear strength to weakening that would be consequential at the scale of the structure.

The capacity of surrounding soils to accommodate losses of shear resistance in the weakening materials is another useable indicator for assessing the potential for uncontained plastic flow. A soil that has begun strain-weakening is unstable and will continue weakening until it reaches residual levels of shear resistance, unless it is externally stabilized by the adjacent materials. If these are at yield (a state captured by local safety factors at or near unity, as demonstrated in Fig. 8), they cannot accommodate the loss of strength to strain-weakening by upward adjustments of stress states and instead experience plastic flow, thus contributing to the expansion of the failure zone. The combined monitoring of reserve shear strengths and of impending changes in the extent of weakening would offer a measure of warning for imminent failure when the former are largely depleted and the latter is about to increase dramatically.

The aggregate rates of loss and mobilization of shear strength must also be considered on balance. For example, the results of the Mount Polley simulation indicate that the large reserves of shear resistance in the rockfill remained unmobilized owing to lower deformation moduli.

*Reduction in Levels of Mobilized Shear Resistance in the Extending Regions of the Slide*

In the simulation, the upper till, and later the core, accommodate the shearing of the foundation by extending. This eventually triggers a reversal of the stress response whereby the stress states, previously seen to increase in response to the addition of embankment loads, instead experience a sustained decrease during the global failure (Fig. 10a-b). An examination of the stress responses in the affected zones suggests that the progressive reduction in the levels of shear resistance along the planes of critical stress is driven by the reduction of minor principal stresses. This response can arise from either a loss of confinement or tensile failure.

The possibility of tensile failure in the extensional zone of the slide should be given consideration. In the Mount Polley case study, the presence of numerous open and debris-filled cracks in the core and upper till in the upstream region of the slide (documented by IRP 2015, Appx. C, and KCB 2015, p. 19) suggests this possibility. The laboratory testing data of these units do not support strength models with a tensile component (KCB 2015, pp. 23-25; IRP 2015), and so this mode of failure was not built into the simulation inputs. Nevertheless, the reduction in the levels of mobilized shear resistance following tensile failure in the extensional regions of a slide is a credible mechanism that merits consideration in the context of other slope stability problems.

*Differential Mobilization of Shear Strength Owing to Stiffness Incompatibility*

The presence of stiffness incompatibility issues in the Mount Polley embankment was suggested by two pieces of evidence: compaction issues in the shell zone, and the deformation of the rockfill at the breach location.

The deformation of the shell zone stood in contrast with the brittle responses to shearing documented in the core and foundation. The rockfill deformed considerably, shifting in the downstream direction by ~20m, reaching and in places surpassing the toe of the slide (Fig. 4b, feature R; IRP 2015, Fig. C3.5.7). Multiple consecutive echelon scarps were documented at its face (IRP 2015, Appx. C).

The relatively ductile deformation-stress response of the rockfill at Mount Polley is typical for this class of materials. Leps (1970) reports from observations on large-cell triaxial tests that at low confining stresses, the axial straining characteristics of rockfills change considerably as a function of confinement, and that this behavior is more pronounced in poorly compacted samples. The results reported by Leps (1970) indicate a direct correlation between confining stresses and deformation moduli. Deformation moduli derived from tests conducted at low confining stresses are rather low, especially in uncompacted or poorly compacted rockfills. At Mount Polley, issues with compaction have been noted where construction records specify lifts with an excessive thickness as well as end-dumping at the face in the later construction stages (KCB 2015, p. 7). If the correlations reported by Leps (1970) apply here, a full mobilization of shear strength would require an appreciable deformation of this material. In his comprehensive review of rockfill properties, Marsal (1973, p. 195) notes that such a response is to be expected in rockfills and must be integrated into stability evaluations.

The stiffness incompatibility issues in the Mount Polley slope were accommodated in the numerical analysis through appropriate modeling inputs, and the effects were monitored by tracking the stress states throughout the domain and especially in the shell zone. A sensitivity assessment of variable deformation properties undertaken by Zabolotnii (2020, pp. 144-147) shows that strain compatibility issues are prevalent throughout.

**Three-Dimensional Slope Stability Effects in the Mount Polley Failure**

In the numerical analysis of the embankment failure at Mount Polley, the collapse initiates when the weakening in the Upper GLU is relatively modest, with the strain-weakening zone encompassing an area of ~1,800m$^2$ (representing ~1/10 of its total area in the failure zone of ~16,000m$^2$), and with an average reduction of strength across it <8% (Fig. 7b). This determination stands in contrast with the results of the three-dimensional limit equilibrium analyses, suggesting that the collapse can be triggered only upon the reduction of shear resistance to residual values across the entire Upper GLU area involved in failure. A three-dimensional limit equilibrium safety factor using an 8% reduction of strength from peak across ~1/10 of the Upper GLU area involved in failure would be only marginally lower than the value calculated using peak undrained resistance, of ~1.3.

The above, in conjunction with the findings in the results section, lead to the conclusion that the three-dimensional stability effects identified in the slope at Mount Polley by means of limit equilibrium analysis are partly nominal, with the shear strength of the rockfill only partially mobilized at the start of collapse, and partly offset by the reduction of the mobilized shear resistance in the upper till and core in the upstream region of the slide that is not captured by this type of analysis. In other words, the three-dimensional limit equilibrium analysis of this failure is nonconservative because of inadequate representation of mobilized shear resistance in the rockfill as well as material experiencing stress reductions due to the deformations. This finding strengthens the conclusion that limit equilibrium methods are unsuited for evaluations of progressive failure.

## CONCLUSION

This paper demonstrates that limit equilibrium analysis is unsuited for evaluating progressive failures. Each of the three mechanisms of progressive failure identified in the Mount Polley case study is deformation-dependent and therefore not amenable to evaluation by means of limit equilibrium methods. The simplification of limit equilibrium methods which precludes the capture of asynchronous mobilization of shear resistance resulting from these mechanisms may introduce a nonconservative error into the safety factor calculations.

There is a growing recognition by the geotechnical community that all slope failures are progressive to some degree, i.e., they experience an asynchronous mobilization of shear strength, if only due to nonuniform distributions of strains and stresses. This view is supported by the findings in this paper, as two mechanisms of asynchronous mobilization of shear strength identified here, owing to stiffness incompatibility and to loss of confinement, may be present in the absence of strain-weakening.

Historically, geotechnical engineers have relied on limit equilibrium analysis while recognizing its limitations, including those related to its application to progressive failure. In the absence of better methods, the use of limit equilibrium analysis was necessary. With recent advancements in computational geomechanics, the example presented here is supportive of the increased utilization of deformation-based numerical analysis in geotechnical analysis of slope behavior. The case study of the failure of the Mount Polley embankment demonstrates that the strength of the numerical analysis lies not with its ability to produce safety factor calculations that are comparable to those obtained by limit equilibrium analyses, but with its potential to capture the stress path of a structure and, in doing so, to offer clues about the risks of instability associated with credible stress paths.

## ACKNOWLEDGMENTS

The authors extend their gratitude for the financial support of this research to the Vanier Graduate Scholarships Program, the Natural Sciences and Engineering Research Council of Canada (NSERC), and Alberta Innovates – Clean Energy. They acknowledge the significant role that the two initial investigators of failure at Mount Polley, the Independent Expert Engineering Investigation and Review Panel and Klohn Crippen Berger, played in developing the knowledge base for this research. The authors thank Itasca Consulting Group, Ltd., for providing FLAC3D software free of charge for this project under their educational partnership program. Their gratitude is extended to Augusto Lucarelli, principal with Itasca, for his mentorship through some of the modeling aspects of this research.

## DATA AVAILABILITY

Select models, results, and code generated or used during the study are available in the online repository found at https://doi.org/10.20383/102.0475.

## ABBREVIATIONS

| | |
|---|---|
| *DSS* | direct simple shear |
| *FEM* | finite element method |
| *FS* | safety factor |
| $FS_{local}$ | local safety factor, defined in equation 1 |
| *LEM* | limit equilibrium method |
| *mASL* | meters above sea level |
| *MPMC* | Mount Polley Mining Corporation |
| *OCR* | overconsolidation ratio |
| *SSI* | stress-strain incompatibility |
| *SSR* | shear strength reduction |
| *TSF* | Tailings Storage Facility |

## REFERENCES


CDA, 2014. "Technical Bulletin: Application of Dam Safety Guidelines to Mining Dams." Canadian Dam Association, 43 pages.

Golder, H.Q., and D.J. Palmer (1955). "Investigation of a bank failure at Scrapsgate, Isle of Sheppey, Kent." Géotechnique 5(1): 55-73.

Independent Expert Engineering Investigation and Review Panel (IRP). "Report on Mount Polley Tailings Storage Facility Breach." Government of British Columbia, January 30, 2015. 147 pages.

Jefferies, M., N.R. Morgenstern, D. Van Zyl and J. Wates. "Report on NTSF Embankment Failure, Cadia Valley Operations for Ashurst Australia." Report No. H356804-00000-22A-230-0001. April 17, 2019.

Klohn, Crippen and Berger (KCB). "Mount Polley tailings dam failure – Assessment of failure mechanism." Report no. M09954A01.730. BC Ministry of Energy and Mines, May 2015. 978 pages.

Ladd, C. (1991). "The Twenty-Second Karl Terzaghi Lecture: Stability evaluation during staged construction." Journal of Geotechnical Engineering, 117(*4*): 540-615.

Leps, T.M. (1970). "Review of shearing strength of rockfill." In Proceedings of American Society of Civil Engineers, J. Soil Mechanics and Foundations Division Vol. 96: 1159-1170.

Marsal, R.J. (1973). "Mechanical properties of rockfill." Embankment Dam Engineering, Casagrande Vol., 109-200. New York: Wiley. Accession Number: 00096416.

Ministry of Energy and Mines (MEM), Mining and Mineral Resource Division. "Investigation Report of the Chief Inspector of Mines: Mount Polley Mine Tailings Storage Facility Breach." Ministry of Energy and Mines, Govt. of British Columbia. November 30, 2015. 188 pages.

Moore, I.D. and R.K. Rowe. (1988). "Numerical models for evaluating progressive failure in earth structures – a review." Computers and Geotechnics 6: 217-239.

Morgenstern, N.R., S.G. Vick, C.B. Viotti and B.D. Watts. "Report on the immediate causes of the failure of the Fundão dam." August 25, 2016, Report, 76 pages.

Potts, D. M., Dounias, G. T. & Vaughan, P. R. (1990). "Finite element analysis of progressive failure of Carsington embankment." Géotechnique, 40(*1*): 79-101.

Quinn, J., B. Chin, M. Pernito and J. Scammell. "Geotechnical assessment of Alameda Dam." GeoRegina, Sep. 28- Oct. 1 2014, Regina, Canada.

Skempton, A.W. (1964). "Fourth Rankine Lecture: Long-Term Stability of Clay Slopes." Géotechnique, 14(2): 77-102.

Taylor, D.W. "Fundamentals of soil mechanics." Wiley, New York, 8th Printing, 1955. ASIN: B000IN5E3W.

Terzaghi, K. "Stability of slopes of natural clay." In Proceedings, 1st Intl. Conf. Soil Mech., Harvard, Massachusetts, 1936, Vol. 1: 161-165.

Terzaghi, Karl, and Ralph B Peck. "Soil Mechanics In Engineering Practice." New York: J. Wiley, 1948.

Zabolotnii, Elena. "Three-dimensional slope stability effects in the failure at the Mount Polley Tailings Storage Facility." PhD Thesis. University of Alberta, Edmonton, Canada, 2020.

Zabolotnii, Elena. "Select results: the deformation back-analysis of the failure of the Mount Polley TSF embankment." Dataset, https://doi.org/10.20383/102.0475.

Zabolotnii, E., Morgenstern, N.R. and G.W. Wilson (2021). "Mesh sensitivity in numerical models of strain-weakening systems." Computers and Geotechnics 136, https://doi.org/10.1016/j.compgeo.2021.104253.


## NOTATIONS

$K_0$ – coefficient of at-rest lateral pressure
$s_{cr}$ – mobilized shear stress on the critical plane
$s_u$ – undrained shear strength
$\tau_{ff}$ – shear strength on the critical plane
$\gamma_s^p$ – plastic shear strain

The open access Mission of the International Journal of Geoengineering Case Histories is made possible by the support of the following organizations:






Access the content of the ISSMGE International Journal of Geoengineering Case Histories at:
https://www.geocasehistoriesjournal.org

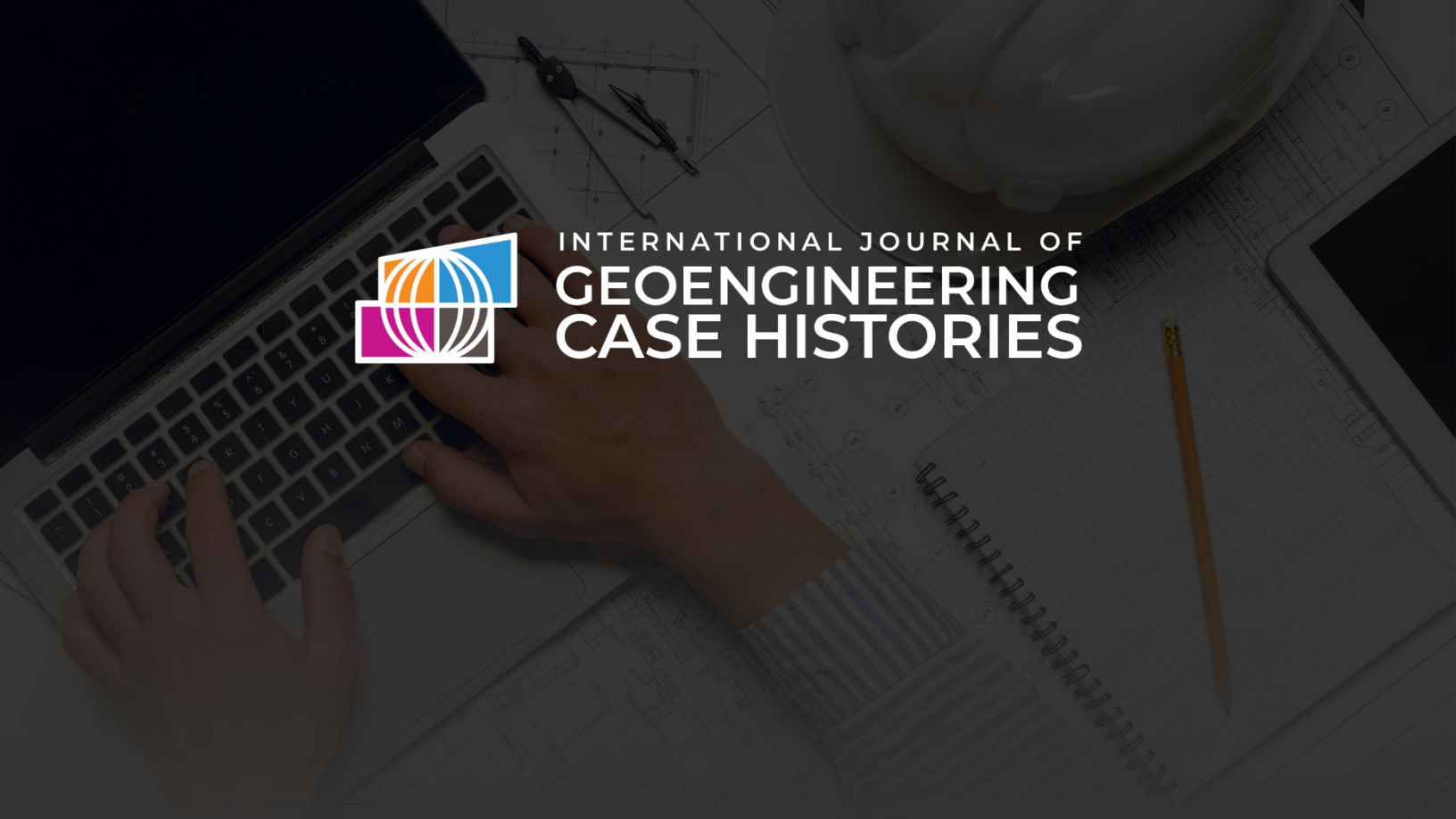

INTERNATIONAL JOURNAL OF
GEOENGINEERING
CASE HISTORIES

***The Journal's Open Access Mission is generously supported by the following Organizations:***